

Small angle neutron scattering and calorimetric studies of large unilamellar vesicles of the phospholipid dipalmitoylphosphatidylcholine

P. C. Mason and B. D. Gaulin

Department of Physics and Astronomy, McMaster University, Hamilton, Ontario, Canada L8S 4M1

R. M. Epan

Department of Biochemistry, McMaster University, Hamilton, Ontario, Canada L8N 3Z5

G. D. Wignall and J. S. Lin

Center for Small-Angle Scattering Research, Oak Ridge National Laboratory, Oak Ridge, Tennessee 37831

(Received 14 September 1998)

High-resolution differential scanning calorimetry (DSC) and small angle neutron scattering (SANS) experiments have been conducted on large unilamellar vesicles (LUV's) of the phospholipid dipalmitoylphosphatidylcholine (DPPC) in excess water. The DSC results indicate a phase transition at temperatures corresponding to the gel ($L_{\beta'}$) to ripple ($P_{\beta'}$) phase transition seen in multilamellar vesicles of DPPC while the SANS experiments provide direct evidence for the formation of the $P_{\beta'}$ phase in these systems. In addition, it is shown that SANS is an effective technique for extracting structural parameters such as vesicle radius and thickness in LUV model membrane systems. [S1063-651X(99)02103-0]

PACS number(s): 87.16.-b, 61.12.Ex, 07.20.Fw

I. INTRODUCTION

Phospholipids such as dipalmitoylphosphatidylcholine (DPPC) have been the object of intense study due to their unique physical properties, rich phase behavior, and role as model membrane systems analogous to more complex biological membranes. Large unilamellar vesicles (LUV's), in particular, mimic well their counterparts in nature, consisting of a single lipid bilayer forming a closed membrane encapsulating an aqueous core. Characterization of LUV properties such as vesicle radius and bilayer thickness have typically been done using dynamic light scattering [1–4]. While this technique has been and will continue to be an invaluable tool in the study of LUV's, it is important to develop complementary approaches that may prove useful for elucidating the salient features of LUV systems under a variety of experimental conditions such as, for example, lipid systems with inserted membrane proteins and peptides. Small angle neutron scattering (SANS) is such a technique. In this paper we will show that SANS is sensitive to LUV morphology and present evidence for the existence of the ripple phase in unilamellar vesicles of DPPC.

The ripple $P_{\beta'}$ phase of DPPC, first discovered by Tardieu, Luzzati, and Reman [5], is a well-studied phase in which the lipid bilayer develops a periodic spatial modulation. Despite this attention, many issues concerning the ripple phase remain unresolved. Several theoretical models of the $P_{\beta'}$ phase propose that the ripple structure is a result of lipid-lipid interactions within the bilayer [6–8]. However, while this phase forms readily in multilamellar vesicles (MLV's) of DPPC, compelling evidence for its formation in LUV's does not exist. Previous differential scanning calorimetry (DSC) studies [9–11] on DPPC LUV's have suggested the existence of the gel, $L_{\beta'}$, to $P_{\beta'}$ transition (known as the pretransition) with evidence of small enthalpy

changes at temperatures corresponding to the pretransition temperature in MLV's.

Observations by Fang and Yang [12] using atomic force microscopy (AFM) show a rippled structure in the upper layer of supported double bilayers of DPPC while regions of the same sample with only a single bilayer covering show no signs of a ripple, supporting theories that bilayer-bilayer interactions may also play an integral part in the formation of a rippled structure [13]. The absence of ripples in domains of single bilayers in the Fang and Yang [12] study may be the result of suppression of undulations due to the substrate although rippled structures have been observed in single bilayers using AFM both with supported asymmetric unilamellar bilayers [14] (in which the opposing leaflets of the bilayer are composed of different lipids) and with supported unilamellar bilayers of DPPC in the presence of certain chemical compounds [15]. While these studies [12,14,15] should aid in the development of a complete microscopic theory of intralayer and interbilayer interactions, the relevance to the $P_{\beta'}$ phase in vesicular DPPC remains unclear. We present the results of DSC and SANS experiments on DPPC LUV's, which point to the existence of the $P_{\beta'}$ phase in these systems.

II. MATERIALS AND EXPERIMENTAL METHODS

1,2-dipalmitoyl-sn-glycero-3-phosphocholine (DPPC) was purchased from Avanti Polar Lipids, Inc. (Birmingham, AL) and used without any further purification. For the small angle neutron scattering (SANS) experiments, 50 mg of DPPC was suspended in a 0.5-mL D_2O /PIPES buffer (20 mM PIPES, 1mM EDTA, 150 mM NaCl in D_2O adjusted to a pH meter reading of 7.4). This buffer simulates physiological conditions and has the advantage of avoiding potential experimental artifacts caused by marked changes in pH due

to the presence of small amounts of contaminants in an unbuffered solution.

The dispersion was freeze-thawed five times using alternating liquid nitrogen and warm water cycles to promote equilibrium transmembrane distributions of solutes [16]. It is important to avoid transmembrane osmolality variations as such conditions can lead to dramatic differences in vesicle size [3] and morphology [17]. LUV samples were then made by extruding the suspension ten times under nitrogen pressure using a stainless steel extrusion device (Lipex Biomembranes, Inc., Vancouver, B.C.). Each extrusion cycle was performed through two stacked 100 nm pore size polycarbonate filters (Nucleopore Corp., Pleasanton, CA), following the procedure outlined by Hope *et al.* [18]. LUV's prepared in this way are known to be essentially monodisperse [3], almost exclusively unilamellar [18], and extremely stable over periods up to six months [19]. The solution was transferred to a 1-mm path length Helma quartz cell designed for SANS experiments on solutions.

The SANS experiments were conducted at the W.C. Koehler 30 m SANS facility at the Oak Ridge National Laboratory [20] using neutrons of wavelength 4.75 Å ($\delta\lambda/\lambda \sim 5\%$). Three configurations of the instrument were employed with sample to detector distances of 1.5 m ($Q = (4\pi/\lambda)\sin\theta \in [0.035, 0.39 \text{ \AA}^{-1}]$ where 2θ is the scattering angle), 3.2 m ($Q \in [0.017, 0.19 \text{ \AA}^{-1}]$), and 18.0 m ($Q \in [0.003, 0.03 \text{ \AA}^{-1}]$), for relatively low-, medium-, and high-resolution measurements, respectively. The SANS data were corrected for instrumental backgrounds and detector efficiency and converted into absolute differential cross sections per unit sample volume using established protocols [21,22].

Samples for the DSC were prepared by suspending 10.0 mg of DPPC in 10.0 mL of PIPES buffer and following the LUV preparation procedure outlined above. Measurements were made using a Nano Differential Scanning Calorimeter (Calorimetry Sciences Corporation, Provo, UT). The features of the design of this instrument have been previously described [23]. Solutions were degassed under vacuum prior to loading in the calorimeter cells.

III. RESULTS AND DISCUSSION

A. Differential scanning calorimetry

Reported enthalpy changes at the pretransition vary greatly depending on the LUV preparation method, vesicle size, and buffer solution [9–11]. We have conducted DSC experiments on LUV's of DPPC at various scan rates. The results of two different scan rates are displayed in Fig. 1 with the top panel showing data collected at 0.75 °C/min and the bottom data collected at 2.00 °C/min. The solid lines represent fits to the data consisting of a linear background term, a Lorentzian centered at the pretransition temperature, and an inverse power law that describes the low-temperature side of the main transition peak. The fits are cut off just below the main transition temperature as the asymmetry in the main transition peak complicated the analysis without adding to the interpretation. The insets show the data with the background and the contribution of the main transition (the inverse power law) subtracted, along with the Lorentzian contribution to the fit. In both cases there is clear evidence for

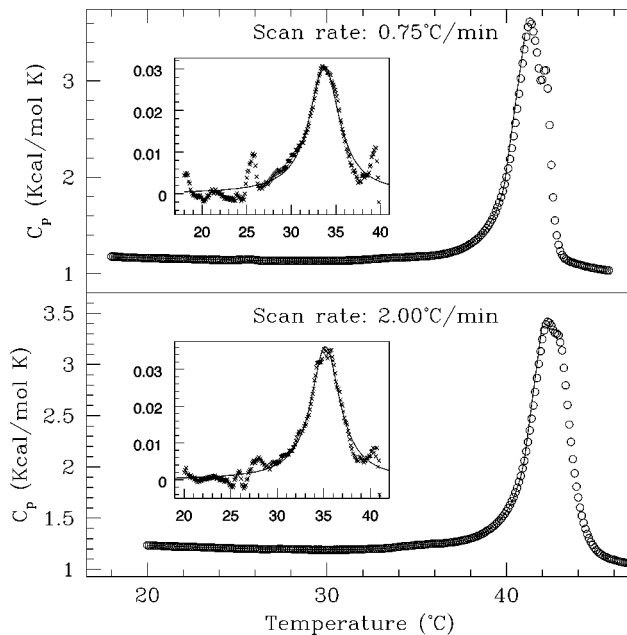


FIG. 1. DSC results at two different scan rates on DPPC LUV's. The solid line is a fit to the data. As described in the text, the insets show the difference between the data and the sum of the background and contribution of the main transition peak at $T \sim 42$ °C. The solid line in the insets is the Lorentzian component of the fit to the data sets. Both scan rates give clear indication of the pretransition. The results of quantitative analysis of the measurements are listed in Table I.

the pretransition with enthalpy changes far in excess of what would be expected even if there was an improbably high amount of multilamellar contamination in the samples. The results of these experiments are summarized in Table I, along with the results of an experiment performed for comparative purposes on a DPPC MLV sample in the same environment. The enthalpy changes and transition temperatures for the MLV sample agree well with known values [24] while the LUV enthalpies are on the low end of the range of those reported in the literature.

B. Small angle neutron scattering

Based on previous results on egg PC [18,25,26] prepared using similar techniques as our own, we expect our LUV samples to be monodisperse, unilamellar, spherical vesicles. From a scattering standpoint, such samples in low concen-

TABLE I. DSC results for DPPC LUV's at two different scan rates and MLV's at a scan rate of 0.75 °C/min. The results presented are from scans as the sample was warmed. The subscripts p and m refer to the pretransition and main transition, respectively.

Sample type	Scan rate (°C/min)	T_p (°C)	ΔH_p (kcal/mol)	T_m (°C)	ΔH_m (kcal/mol)	$\frac{\Delta H_p}{\Delta H_m} (\times 100\%)$
LUV	0.75	33.7	0.16	41.3	7.0	2.3
	2.00	35.2	0.18	42.3	7.2	2.5
MLV	0.75	36.0	1.1	42.0	7.4	15

tration should be easily modeled as hollow, noninteracting spheres for which the scattering function is simply the difference between the Fourier transforms of concentric spheres. This can be written analytically as

$$S(Q) = A \left[\frac{(R+d)^3 \frac{\sin[Q(R+d)] - Q(R+d)\cos[Q(R+d)]}{[Q(R+d)]^3} - R^3 \frac{\sin(QR) - QR\cos(QR)}{(QR)^3} \right]^2, \quad (1)$$

where A is an overall amplitude of the scattering, R is the radius of the LUV, and d is the thickness of the bilayer. The radius is a measure of the membrane curvature, which is an important parameter in membrane elasticity theories (see, for example, [27–33]) and is thought to influence such properties as transbilayer lipid transport processes [34], while the bilayer thickness plays an integral role in modulating the function of transmembrane proteins among other properties [35]. The scattering function given in Eq. (1) can be expanded in terms of products of periodic functions and shown to consist of a rapidly oscillating term with a period of $2\pi/R$ within an envelope of much more slowly varying oscillations of period $2\pi/d$. Thus, we expect that we should be able to extract these membrane parameters from scattering data taken over a sufficiently broad range in Q space.

In our SANS experiments, the scattering events actually measured are a convolution of the true scattering function of the system with the appropriate resolution function of the instrumentation:

$$I(Q) = \int_{Q'} S(Q') R(Q-Q') dQ', \quad (2)$$

where $S(Q')$ is the scattering function given in Eq. (1) and $R(Q-Q')$ is the instrumental resolution function centered at Q . A short discussion of resolution function appears in the appendix. Since the SANS intensities are converted to absolute differential cross sections per unit sample volume and the Q ranges from the three different resolution configurations overlap, we are able to assemble the data into a single scattering curve, as shown in Fig. 2, which extends over four and a half decades in measured intensity and almost two decades in Q . The data shown in Fig. 2 were collected at 20 °C, which corresponds to the gel $L_{\beta'}$ phase of DPPC. The best fit to the data, using Eq. (2) and a Gaussian resolution function, was obtained using a nonlinear least squares fitting routine and is shown as the solid line in the figure. The unconvoluted fit appears as the dotted line.

Inspection of Fig. 2 shows that the fit using Eq. (2) under the assumption of a sample of monodisperse, noninteracting, hollow spheres is a good description of the data. The fit describes the data over four decades in intensity and over one and a half decades in Q , yielding a membrane radius of $R = 570 \text{ \AA}$ and thickness $d = 38.4 \text{ \AA}$. Deviations from the fit are seen at small values ($< 0.01 \text{ \AA}^{-1}$) of Q , where the fit falls below the actual scattering. We speculate that this is due to intervesicular contributions to the scattering.

The fit also fails to describe the data well at the major distinguishing feature seen in the data in Fig. 2—the shoulder at $\sim 0.1 \text{ \AA}^{-1}$. The instrumental resolution function

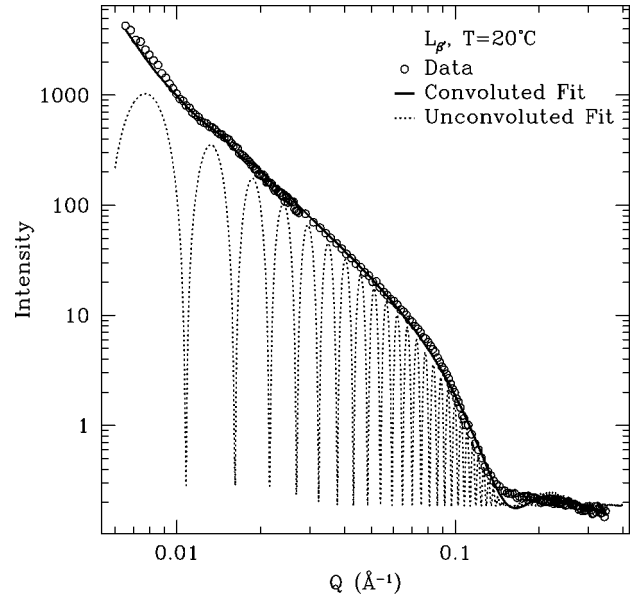


FIG. 2. Fit to the scattering profiles of DPPC LUV's at 20 °C, as described in the text.

smears the data in much the same way as would a polydisperse sample centered about a mean radius and it was found that increasing the width of the instrumental resolution function, $R(Q-Q')$, did not improve the fit in this region. Therefore, it is unlikely that polydispersity would affect the goodness of the fit. The discrepancy cannot be explained by assuming a scattering contribution from a bilayer periodicity, which would occur if there was a small multilamellar component to our samples as such scattering would be apparent in the subtractions of the data sets shown later in this paper. There have been reports of nonspherical LUV's in an isoosmotic environment similar to ours [17]. Deviations from a spherical form could affect our scattering pattern in such a way that it cannot be fully described by the simple form given in Eq. (1). However, given the good overall description of the data over such a wide range of Q and intensity, it is unlikely we are seeing dramatic shape fluctuations such as those described, for example, by Mui *et al.* [17].

While the membrane radius R taken from our fit falls within accepted values for LUV's produced by extrusion [1], the membrane thickness d falls below established values [35,36]. This is not surprising since the location of the shoulder in the SANS profile ($Q \sim 0.1 \text{ \AA}^{-1}$) gives a measure of d and this is precisely where our fit fails to adequately describe the data in detail. The top panel of Fig. 3 shows medium resolution data at temperatures corresponding to the gel ($L_{\beta'}$, $T = 20 \text{ °C}$) ripple ($P_{\beta'}$, $T = 37 \text{ °C}$), and liquid crystalline (L_{α} , $T = 50 \text{ °C}$) phases, highlighting the region in which the shoulder seen in Fig. 2 occurs. In this region of Q space, there is no discernible difference between the data sets collected at 20 and 37 °C, which is expected even if the sample is in the $P_{\beta'}$ phase at 37 °C since both the $L_{\beta'}$ and $P_{\beta'}$ phases are gel phases with the acyl chains being largely trans rotomers. Thus, a change in membrane thickness and subsequent shift in the shoulder feature would be surprising. In the L_{α} phase at $T = 50 \text{ °C}$, the rotational isomerism associated with the melting of the acyl chains leads to a decrease in membrane thickness, pushing the shoulder out to a higher

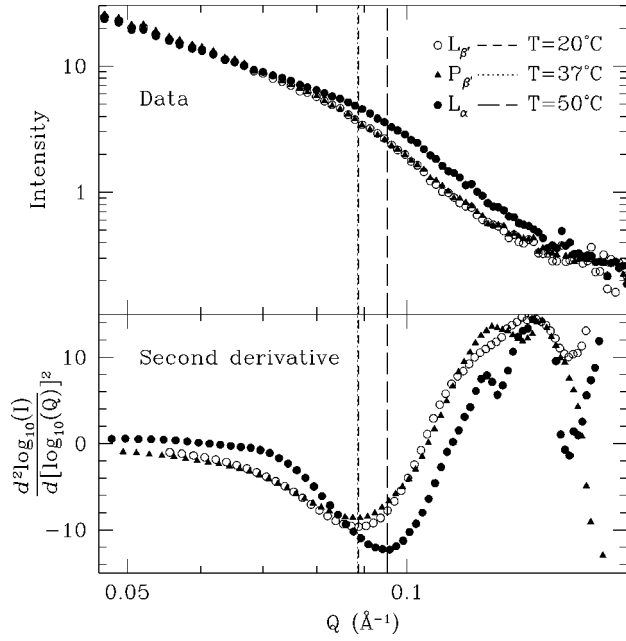


FIG. 3. Results of medium resolution SANS LUV experiments: the top panel shows data collected at temperatures corresponding to the $L_{\beta'}$, $P_{\beta'}$, and L_{α} phases while the bottom panel shows the curvature in the data. The vertical lines indicated positions of maximum curvature.

value of Q as is clearly seen in the figure.

The shoulder in the data is a region of local maximum curvature of the plot and will therefore correspond to a local minimum in the second derivative. The bottom panel of Fig. 3 shows the second derivative of the three data sets, along with lines marking the location of the local minimum. The shift in the minimum for the L_{α} phase data clearly corresponds to the shift in the location of the shoulder in the data. We can do the same derivative analysis with the convoluted theoretical scattering function by varying the two membrane parameters systematically, generating the scattering curve numerically, convoluting with the resolution function, and finding the location of the second derivative minimum for each set of input parameters. Repeating this procedure for a wide range of parameters allows us to generate a series of ‘‘calibration curves’’ which relate the position of maximum curvature, the shoulder, to the membrane thickness d for a given value of the vesicle radius R .

Using values for the vesicle radii extracted from fits to the joined data over the three different resolutions such as that shown in Fig. 2, a calibration curve of shoulder position versus membrane thickness was generated, as shown in Fig. 4, for each of the three temperatures measured. Horizontal lines from the three Q values corresponding to maximum curvature taken from the data in Fig. 3 are shown in Fig. 4. These lines intercept their corresponding calibration curves at which point a line can be dropped to the abscissa, yielding a value for the membrane thickness d for each temperature. The results of this analysis yield $d_{L_{\alpha}} = 45 \pm 2$, $d_{P_{\beta'}} = 50 \pm 2$, and $d_{L_{\beta'}} = 50 \pm 2$ Å. It is these values of the membrane thickness, well within the range of accepted values [36], that we believe accurately represent the information provided by our SANS data. Uncertainties regarding these values are estimated by varying R in the theoretical fits to the point that

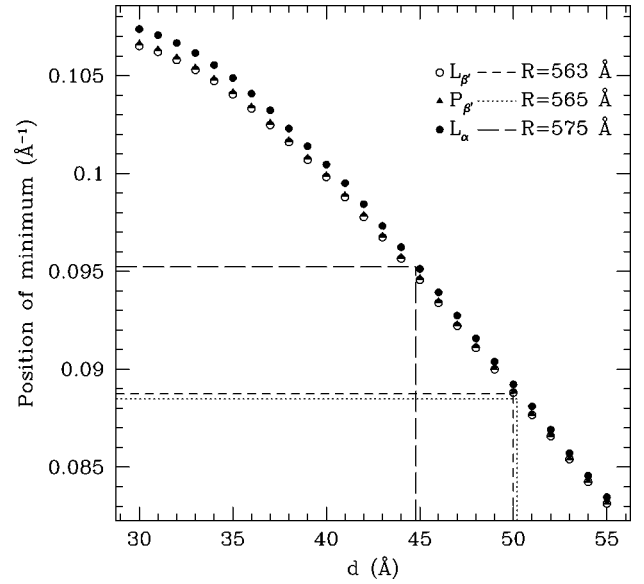


FIG. 4. Calibration curves relating the position of the minimum in the second derivative of the convoluted theoretical scattering function [Eq. (2)] to the membrane thickness d as it appears in Eq. (1). The dashed lines correspond to minimums in the second derivative of the SANS data, taken from Fig. 4, which are used to extract an accurate estimate of d in each phase.

they no longer describe the data well. A membrane thickness based on these limiting values of R is considered to be a fair indication of the uncertainty in d . The results of the fitting and derivative analysis are summarized in Table II. While the results of the two analyses differ significantly in their absolute values for the membrane thickness, it is interesting to note that both are consistent in showing that d does not change (within uncertainty) in going from 20 to 37 °C, while it decreases by $\sim 12\%$ in the L_{α} phase, in agreement with measurements using other techniques.

As evidenced by Fig. 2, resolution limited measurements of the scattering function given by Eq. (2) show relatively few features. The shoulder in the data at $Q \sim 0.1$ Å $^{-1}$, discussed above, corresponds to the slowly varying oscillations of period $2\pi/d$. At small Q , the more rapid $2\pi/R$ oscillations can be probed. The upturn in the data at $Q \sim 0.012$ Å $^{-1}$ will give a measure of these high-frequency oscillations. From the results given in Table II, using fitting routines to determine the vesicle radius gives nearly identical values for R at 20 and 37 °C. While the fits are not particularly sensitive to small changes in R , subtractions of the data should highlight any differences present in the sample due to

TABLE II. Vesicle parameters as determined by SANS analysis. The first column of vesicle thickness d values were extracted from fits to the data, while the second were determined by derivative analysis and are the accurate absolute measure of d . R is the vesicle radius.

Temp. (°C), phase	R (Å)	$d_{fit} \pm 0.4$ (Å)	$d_{deriv} \pm 2$ (Å)
20, $L_{\beta'}$	563 ± 12	39.6	50
37, $P_{\beta'}$	565 ± 12	39.3	50
50, L_{α}	575 ± 12	35.5	45

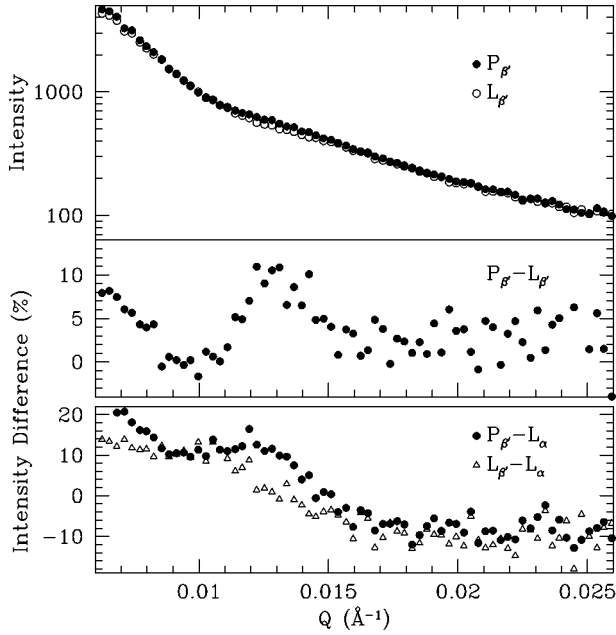


FIG. 5. High-resolution LUV SANS curves: the top panel shows profiles taken in the $P_{\beta'}$ and $L_{\beta'}$ phases with the difference in the curves appearing below; the bottom panel shows the difference between scattering in the L_{α} phase and in the $P_{\beta'}$ and $L_{\beta'}$ phases, respectively.

the change in temperature. A shift in R should result in an observable difference between the data sets at small Q , on the order of $2\pi/R \sim 2\pi/500 = 0.0125 \text{ \AA}^{-1}$. The top panel of Fig. 5 shows high-resolution data taken at temperatures corresponding to the $L_{\beta'}$ and $P_{\beta'}$ phases. The middle panel shows a subtraction of the data sets in the top panel, which peaks at $Q \sim 0.013 \text{ \AA}^{-1}$. The bottom panel of Fig. 5 shows subtractions of the remaining two data sets. The $P_{\beta'}$ set minus the L_{α} set peaks at $Q \sim 0.012 \text{ \AA}^{-1}$ while the $L_{\beta'}$ minus the L_{α} peaks weakly at $Q \sim 0.011 \text{ \AA}^{-1}$. Thus, while the fitted values of the vesicle radius given in Table II are indistinguishable within error, the data subtractions clearly show sensitivity to relative shifts in R in each of the three phases.

Similar subtractions of the medium resolution data are shown in Fig. 6. It is very interesting to note that the subtraction of the $L_{\beta'}$ phase data from the data collected at $T = 37^\circ\text{C}$ shows a 5% difference in the scattering peaking at $Q \sim 0.055 \text{ \AA}^{-1}$. The subtraction of the L_{α} data from the $T = 37^\circ\text{C}$ (bottom panel) also peaks at this same wave vector, whereas the subtraction of the L_{α} phase from the $L_{\beta'}$ phase shows a negligible difference in scattering at this value of Q . The peak in the intensity differences at $Q \sim 0.055 \text{ \AA}^{-1}$ cannot be explained by differences in either vesicle radius or thickness. It can be explained, however, by assuming the development of a ripple structure of wavelength $\lambda_r \sim 115 \text{ \AA}$ in the membrane, direct evidence that the $P_{\beta'}$ phase does indeed form in LUV's of DPPC. If the difference in the data sets is done as a straight subtraction (not shown) as opposed to a percentage difference, one finds that the expected ripple wavelength shifts up slightly giving $\lambda_r \sim 125 \text{ \AA}$. Both of these values for λ_r fall within accepted values for the ripple wavelength for the $P_{\beta'}$ phase seen in DPPC MLV's [38–40]. The large dip in the intensity difference at $Q \sim 0.11 \text{ \AA}^{-1}$ seen in the bottom panel of Fig. 6 is

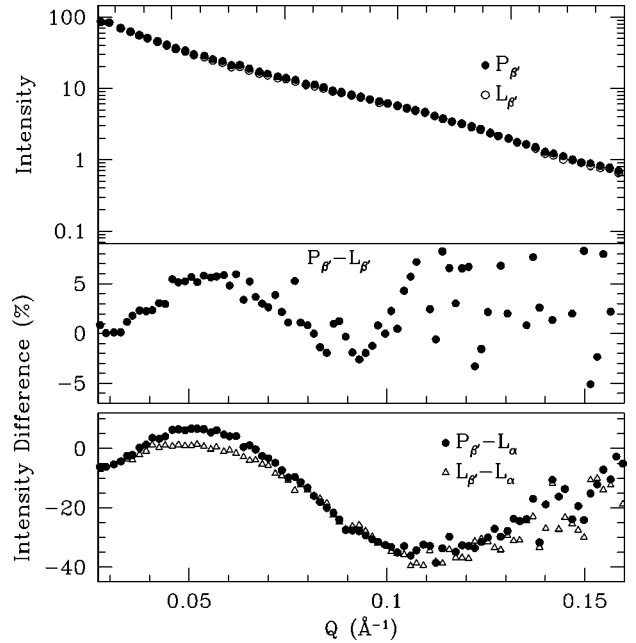


FIG. 6. Medium-resolution LUV SANS curves: the top panel shows profiles taken in the $P_{\beta'}$ and $L_{\beta'}$ phases with the difference in the curves appearing below; the bottom panel shows the difference between scattering in the L_{α} phase and in the $P_{\beta'}$ and $L_{\beta'}$ phases, respectively.

due to the shift in the shoulder position L_{α} phase (cf. Fig. 3) and gives a measure of the order of d . Note that none of the subtractions give evidence for a multilamellar component to our LUV's, as such contamination would yield peaks in the range $0.08 < Q < 0.10 \text{ \AA}^{-1}$.

It is not surprising that the ripple feature of the LUV $P_{\beta'}$ phase should be difficult to see with diffraction. In MLV's, the rippling of the membrane surface occurs in each bilayer of the stacked bilayer construct, forming coherently between bilayers creating a three-dimensional, monoclinic lattice readily apparent in scattering experiments [40]. In LUV's, ripples in the solitary bilayer of each vesicle will contribute incoherently to the scattering in contrast to the coherent contribution to the scattering from multiple rippled bilayers in each MLV. Therefore, the 5% increase in scattering at the ripple wave vector in LUV's in the $P_{\beta'}$ phase, while small compared to the increase seen in MLV's, should not be interpreted as the result of incomplete formation of this phase in LUV's, but rather as a natural suppression of similar scattering seen in MLV systems.

It is interesting to note that we see very little change in vesicle size in going from the $L_{\beta'}$ to the $P_{\beta'}$ phase, contrary to what is seen in MLV systems [37]. There have been reports [41] of marked decreases (as high as 28%) in MLV radius upon entry into the $P_{\beta'}$ phase. We would be sensitive to such changes if they were occurring in our LUV system, suggesting that bilayer-bilayer interactions may play a role in these changes in MLV's.

IV. CONCLUSION

In summary, we show high-resolution differential scanning calorimetry results indicating a small excess heat capacity in DPPC large unilamellar systems at a temperature

where the gel to ripple phase transition is expected in MLV systems. Complimentary small angle neutron scattering experiments were performed on identically prepared large unilamellar vesicles of DPPC at three different temperatures, corresponding to the $L_{\beta'}$, $P_{\beta'}$, and L_{α} phases, at three different instrumental resolutions. We have shown that our samples are well-modeled by monodisperse, unilamellar, noninteracting, hollow spheres and extract reasonable values for both the vesicle radius and membrane thickness from our analysis. We present, for the first time, diffraction evidence for the existence of the $P_{\beta'}$ phase in DPPC LUV's with a ripple wavelength of the same order as seen in MLV systems.

ACKNOWLEDGMENTS

The authors would like to thank R.F. Epand for helpful discussions about the DSC work. This work was supported in part by the Natural Sciences and Engineering Research Council of Canada, and by the Medical Research Council of Canada under Grant No. MT-7654. The research at Oak Ridge was supported by the Division of Materials Sciences, U.S. Department of Energy under Contract No. DE-AC05-

960R22464 with Lockheed Martin Energy Research Corporation.

APPENDIX: DISCUSSION OF THE RESOLUTION/ CONVOLUTION

The choice of resolution function was not critical as the rapid oscillations in $S(Q)$ [see Eq. (1) and Fig. 2] will smear out quickly for any reasonable (finite) choice of instrumental resolution, especially in the medium- and low-resolution configurations. A Gaussian function was chosen since it is simple to model and it has been shown to be a good descriptor of the resolution function for SANS instruments such as those at ORNL [42]. The widths of the resolution function at sample-to-detector distances of 1.5, 3.2, and 18.0 m were 0.024, 0.015, and 0.0065 \AA^{-1} , respectively, based on measurements of widths from resolution-limited Bragg peaks seen in an experiment on multilamellar vesicles of DPPC in the solid $L_{\beta'}$ and $P_{\beta'}$ phases under identical experimental conditions [40,43]. At the boundaries between the data sets care was taken to ensure that the convoluted fit function remained continuous. The parameters extracted from the fits were robust with respect to small variations of the resolution function in all three instrumental configurations.

-
- [1] D. G. Hunter and B. J. Frisken, *Biophys. J.* **74**, 2996 (1998).
 [2] F. R. Hallett, J. Watton, and P. H. Krygsman, *Biophys. J.* **59**, 357 (1991).
 [3] G. White, J. Pencer, B. G. Nickel, J. M. Wood, and F. R. Hallett, *Biophys. J.* **71**, 2701 (1996).
 [4] A. Ertel, A. G. Marangoni, J. Marsh, F. R. Hallett, and J. M. Wood, *Biophys. J.* **64**, 426 (1993).
 [5] A. Tardieu, V. Luzzati, and F. C. Reman, *J. Mol. Biol.* **75**, 711 (1973).
 [6] S. Doniach, *J. Chem. Phys.* **70**, 4587 (1979).
 [7] T. C. Lubensky and F. C. MacKintosh, *Phys. Rev. Lett.* **71**, 1565 (1993).
 [8] J. M. Carlson and J. P. Sethna, *Phys. Rev. A* **36**, 3359 (1987).
 [9] R. Parente and B. Lentz, *Biochemistry* **23**, 2353 (1984).
 [10] R. Parente, M. Hochli, and B. Lentz, *Biochim. Biophys. Acta* **812**, 493 (1985).
 [11] D. Lichtenberg, M. Menashe, S. Donaldson, and R. Biltonen, *Lipids* **19**, 395 (1984).
 [12] Y. Fang and J. Yang, *J. Phys. Chem.* **100**, 15 614 (1996).
 [13] G. Cevc, B. Zeks, and R. Podgornik, *Chem. Phys. Lett.* **84**, 209 (1981).
 [14] D. M. Czajkowsky, C. Huang, and Z. Shao, *Biochemistry* **34**, 12 501 (1995).
 [15] J. Mou, J. Yang, and Z. Shao, *Biochemistry* **33**, 4439 (1994).
 [16] L. D. Mayer, M. J. Hope, P. R. Cullis, and A. S. Janoff, *Biochim. Biophys. Acta* **817**, 193 (1985).
 [17] B. L.-S. Mui, P. R. Cullis, E. A. Evans, and T. D. Madden, *Biophys. J.* **64**, 443 (1993).
 [18] M. J. Hope, M. B. Bally, G. Webb, and P. R. Cullis, *Biochim. Biophys. Acta* **812**, 55 (1985).
 [19] H. Nagano, H. Yao, and K. Ema, *Phys. Rev. E* **51**, 3363 (1995).
 [20] W. C. Koehler, *Physica (Utrecht)* **137B**, 320 (1986).
 [21] G. D. Wignall and F. S. Bates, *J. Appl. Crystallogr.* **20**, 28 (1986).
 [22] W. S. Dubner, J. M. Schultz, and G. D. Wignall, *J. Appl. Crystallogr.* **23**, 469 (1990).
 [23] G. Privalov, V. Kavina, E. Freire, and P. L. Privalov, *Anal. Biochem.* **232**, 79 (1995).
 [24] S. C. Chen, J. M. Sturtevant, and B. J. Gaffney, *Proc. Natl. Acad. Sci. USA* **77**, 5060 (1980).
 [25] R. Nayer, M. J. Hope, and P. R. Cullis, *Biochim. Biophys. Acta* **986**, 200 (1989).
 [26] L. D. Mayer, M. J. Hope, and P. R. Cullis, *Biochim. Biophys. Acta* **858**, 161 (1986).
 [27] W. Helfrich, *Z. Naturforsch. C* **28**, 693 (1973).
 [28] E. A. Evans, *Biophys. J.* **30**, 265 (1980).
 [29] U. Seifert, K. Berndl, and R. Lipowsky, *Phys. Rev. A* **44**, 1182 (1991).
 [30] U. Seifert, *Phys. Rev. Lett.* **70**, 1335 (1993).
 [31] L. Miao, B. Fourcade, M. Rao, M. Wortis, and R. K. P. Zia, *Phys. Rev. A* **43**, 6843 (1991).
 [32] L. Miao, U. Seifert, M. Wortis, H.-G. Döbereiner, *Phys. Rev. E* **49**, 5389 (1991).
 [33] S. Svetina and B. Žekš, *Eur. Biophys. J.* **17**, 101 (1989).
 [34] B. L.-S. Mui, H.-G. Döbereiner, T. D. Madden, and P. R. Cullis, *Biophys. J.* **69**, 930 (1995).
 [35] B. A. Lewis and D. M. Engelman, *J. Mol. Biol.* **166**, 211 (1983).
 [36] Y. Inoko and T. Mitsui, *J. Phys. Soc. Jpn.* **44**, 1918 (1978).
 [37] E. Evans and R. Kwok, *Biochemistry* **21**, 4874 (1982).
 [38] H. Yao, S. Matuoka, B. Tenchov, and I. Hatta, *Biophys. J.* **59**, 252 (1991).
 [39] J. A. N. Zasadzinski, J. Schneir, J. Gurley, V. Ehings, and P. K. Hansma, *Science* **239**, 953 (1988).
 [40] P. C. Mason, B. D. Gaulin, R. M. Epand, G. D. Wignall, and

- J. S. Lin, *Phys. Rev. E* **59**, 921 (1999).
- [41] R. P. Perkins, X. Li, J. L. Slater, P. A. Harmon, P. L. Ahl, S. R. Minchey, S. M. Gruner, and A. S. Janoff, *Biochim. Biophys. Acta* **1327**, 41 (1997).
- [42] J. S. Pedersen, D. Posselt, and K. Mortensen, *J. Appl. Crystallogr.* **23**, 321 (1990).
- [43] P. C. Mason, B. D. Gaulin, R. M. Eband, G. D. Wignall, and J. S. Lin (unpublished).